Height, but not binding epitope, affects the potency of synthetic TCR agonists

Kiera B. Wilhelm[1], Shumpei Morita[1], Darren B. McAffee[1], Sungi Kim[1], Mark K. O'Dair[1], Jay T. Groves[1]*

[1] Department of Chemistry, University of California, Berkeley, Berkeley, CA 94720, USA

* To whom correspondence should be addressed. Email: jtgroves@lbl.gov

ABSTRACT

Under physiological conditions, peptide-MHC (pMHC) molecules can trigger T-cell receptors (TCRs) as monovalent ligands, sparsely distributed on the plasma membrane of an antigen-presenting cell. TCR can also be activated by artificial clustering, such as with pMHC tetramers or antibodies; however, these strategies circumvent many of the natural ligand discrimination mechanisms of the T cell and can elicit non-physiological signaling activity. We have recently introduced a synthetic TCR agonist composed of an anti-TCRβ Fab' antibody fragment covalently bound to a DNA oligonucleotide, which serves as a membrane anchor. This Fab'-DNA ligand efficiently activates TCR as a monomer when membrane-associated and exhibits a potency and activation profile resembling agonist pMHC. In this report, we explore the geometric requirements for effective TCR triggering and cellular activation by Fab'-DNA ligands. We find that T cells are insensitive to the ligand binding epitope on the TCR complex, but that length of the DNA tether is important. Increasing the intermembrane distance spanned by Fab'-DNA:TCR complexes decreases TCR triggering efficiency and T cell activation potency. These results establish design parameters for construction of synthetic TCR agonists that are able to activate polyclonal T cell populations, such as T cells from a human patient, in a similar manner as the native pMHC ligand.

INTRODUCTION

T cells play a central role in adaptive immunity by recognizing foreign peptide fragments presented in MHC molecules (pMHC) with their T-cell receptors (TCR). In order to identify a wide range of potential pathogenic peptides, each individual develops a polyclonal repertoire of T cells with distinct TCR genes. In developing thymocytes, the region of the TCR gene that encodes the pMHC recognition site is scrambled, and cells with TCR clonotypes that successfully pass a screening process survive (1). The resulting diversity of TCRs within an individual is critical for successfully conferring adaptive immunity, but presents challenges to the

study of T cell activation because the cognate pMHC that activates a given T cell is generally not known.

Antibodies that bind the TCR and associated CD3 complex (TCR/CD3) readily activate T cells, as measured by cytokine secretion, proliferation, and changes in surface receptor expression (2–6), but this method of stimulation differs from physiological antigen activation. Anti-TCR/CD3 antibodies, as well as widely used pMHC tetramers (7), induce crosslinking of TCR on the T cell surface. This crosslinking is an essential aspect of their activation mechanism; neither pMHC monomer nor monovalent Fab' antibody fragments are active from solution (7–10), and anti-TCR/CD3 antibodies in solution must typically be further crosslinked by secondary antibodies for full activity (11). By contrast, a growing body of evidence indicates that membrane-associated pMHC molecules are highly active as monomers (12–15). Furthermore, at physiological densities of agonist pMHC (0.1-2 μm^{-2}) (16–18), only tens of individual pMHC:TCR ligation events, which are widely spaced within the cell interface, are sufficient to activate T cells (19, 20). At higher agonist pMHC densities (~10 to 250 μm^{-2}), pMHC:TCR complexes form microclusters (21, 22) that further reorganize into the large scale pattern of the immunological synapse (23, 24). But these larger scale organizations at high antigen density are not required for T cell activation (12–15, 20).

We have recently developed a class of synthetic TCR agonists composed of an anti-TCR/CD3 Fab' fragment covalently bound to a DNA oligonucleotide that can uniformly activate polyclonal T cell populations as membrane-associated monomers (25). Like natively monomeric pMHC, Fab'-DNA molecules are inactive from solution at any concentration, but are highly potent when conjugated to a supported lipid bilayer (SLB) via DNA hybridization. Previous work focused on the anti-TCRβ H57-597 Fab'-DNA (H57 Fab'-DNA) and found it to exhibit a similar potency as a strong pMHC agonist (25). Mechanistic studies of TCR triggering suggest that the Fab' binding

epitope on the TCR/CD3 complex (26, 27) and/or the intermembrane spacing established at TCR binding events may impact ligand potency (28–30).

Here we examine a panel of Fab'-DNA constructs that bind three distinct epitopes on the TCR/CD3 complex and have DNA tethers of various lengths (Fig. 1). We synthesized Fab'-DNA ligands derived from the anti-CD3ε 145-2C11 antibody (2C11 Fab'-DNA) and the anti-CD3ε/γ 17A2 antibody (17A2 Fab'-DNA), in addition to the previously reported anti-TCRβ H57 Fab'-DNA (3–5, 26, 31) (Fig. 1b). Both 2C11 and H57 bivalent antibodies are commonly used to activate T cells and bind at or near the reportedly mechanosensitive FG loop of TCRβ (26, 27, 31–33). The 17A2 antibody is less frequently used to activate T cells and has been reported to be less potent due to its binding geometry to the TCR/CD3 complex (26, 27). DNA tethers ranging from 16 to 76 nucleotides were designed for all Fab's, creating 14 to 50 nm space between apposed membranes at binding events (Fig. 1c). This range of sizes spans from the native pMHC:TCR intermembrane spacing of about 14 nm (34–36) to beyond the spacing of about 30 nm established by ICAM-1:LFA-1 adhesion complexes (37) and the large 21-40 nm extracellular domain of CD45 (38–40), which has long been thought to be sterically excluded by the short pMHC:TCR complex size at T cell – antigen presenting cell junctions (21, 28, 36, 41).

We find that the intermembrane space established by DNA tether length dramatically affects Fab'-DNA potency, with larger spacing leading to less potent cellular activation, but that varying the Fab' binding epitope has essentially no effect. T cell activation was monitored by imaging translocation of a fluorescent reporter for the nuclear factor for the activation of T cells (NFAT) from the cytosol to the nucleus (19, 20, 25). Localized formation of protein condensates of linker for the activation of T cells (LAT) also showed the same trend. LAT is an intrinsically disordered protein that serves a signaling scaffold immediately downstream of TCR triggering (42, 43) and its condensate formation proximal to individual Fab'-DNA:TCR complexes is an

indicator of local signaling activity (44, 45). Overall, the dependency of T cell signaling on linker spacing observed here is consistent with early experimental studies of pMHC size effects (36, 46) and subsequent physical models of TCR activation implicating a role for intermembrane spacing (28–30, 41, 47). These results are also consistent with early studies of similarly-structured bispecific T cell engagers (BiTEs) that show BiTEs are more effective if they bind epitopes creating smaller intermembrane spaces where they bridge TCRs on a T cell to melanoma markers on an opposing cell (48). The T cells' indifferent response to ligand binding epitope suggests that any intramolecular aspects of the TCR triggering mechanism (27, 33, 49) do not strongly depend on TCR engagement geometry, in the context of adhesion molecules and a cell-cell interface.

MATERIALS AND METHODS

Fab'-DNA synthesis

All antibodies were digested with pepsin or Glu-C endoproteinase to retain the cysteines in the hinge region and then partially reduced with cysteinamine to form Fab' fragments. Maleimide-functionalized, dye-labeled DNA oligonucleotides were then conjugated to the free cysteine on the Fab' to form crude Fab'-DNA. This product was purified by size exclusion and ion exchange chromatography to obtain monomeric Fab' conjugated to a single DNA oligonucleotide that was labeled with a single fluorophore (25).

Supported Lipid Bilayer Preparation

Low-defect, fluid supported lipid bilayers (SLB) were prepared from a solution of small unilamellar vesicles (SUVs). SUVs were first prepared by mixing 95% choline (DOPC), 3% maleimide (MCC-DOPE), and 2% Ni^{2+} chelating nitrilotriacetic acid (Ni-NTA-DOGS) headgroup phospholipids in chloroform in a piranha-etched flask, drying and resuspending lipids in Milli-Q water to 0.5 mg/mL total lipid concentration, and sonicating with a probe sonicator. The SUVs were then centrifuged to remove titanium particles and lipid aggregates and mixed 1:1 with 1x

PBS, resulting in a spreading solution with a final concentration of 0.25 mg/mL total lipid content. Supported membranes were formed by vesicle fusion of SUVs by adding this spreading solution to imaging chambers assembled with freshly piranha-etched glass coverslips. Thiol-DNA, complementary to the Fab'-DNA strand, was reduced for 90 min and then incubated on the bilayer at about 1 μM in PBS to obtain a density of approximately hundreds of molecules/μm^2 on the SLB (50). These bilayers were stable overnight at 4 °C. Proteins to be coupled to the bilayer were prepared in imaging buffer, added to the imaging chamber, and incubated for 35 min. Fab'-DNA incubation concentrations ranged from 50 pM for single molecule studies to 10 nM for high density samples. ICAM-1 was incubated at a concentration of 100 nM.

T cell harvesting and culture

CD4+ T cells expressing the AND TCR (51) were harvested, cultured, and transduced as previously described (15, 52). Briefly, T cells were harvested from hemizygous transgenic mice from the cross of (B10.Cg-Tg(TcrAND)53Hed/J) x (B10.BR-H2k2 H2- T18a/SgSnJ) strains (The Jackson Laboratory, Bar Harbor, ME) and activated by moth cytochrome c peptide (MCC_{88-103}) immediately after harvest. IL-2 was added the following day within 24h of the harvest. Cells prepared for live cell assays were retrovirally transduced with NFAT-,mCherry, LAT-eGFP, or a LAT-eGFP P2A NFAT-mCherry plasmid-containing supertatants collected from Platinum-Eco cells (Cell Biolabs, San Diego, CA). T cells were imaged on days 5-8. Cell health was verified each day that data were collected by assessing cell morphology and signaling in response to bilayers with no agonist ligand and high density of pMHC. All animal work was approved by Lawrence Berkeley National Laboratory Animal Welfare and Research Committee under the approved protocols #17702 and #17703.

Microscopy

Imaging experiments were performed on an inverted Nikon Eclipse Ti-E motorized inverted microscope (Nikon, Tokyo, Japan) with total internal reflection fluorescence (TIRF) microscopy,

reflection interference contras microscopy (RICM), and epifluorescence capabilities and laser lines at 405, 488, 532, and 640 nm. Freely diffusing, single Fab'-DNA-Atto647 molecules were imaged in TIRF using 20 ms exposure time, 8.6 mW power at sample, and 1000 gain. Single binding events between Fab'-DNA and TCR were imaged using 500 ms exposure time, 0.4 mW power at sample, and 1000 gain. RICM and epifluorescence images were acquired with moderate exposure time (~100 ms) with gain depending on the intensity of the signal. LAT was imaged using low power (0.4-0.8 mW at sample), moderate exposure time (50-200 ms) and 1000 gain, with exact parameters depending on the expression of LAT-eGFP. Micromanager was used to automate acquisitions and collect data (53).

Image analysis

Single particle data – both freely diffusing Fab'-DNA and ligand bound to TCR – were tracked in the TrackMate plugin of ImageJ (54) and processed using custom MATLAB scripts. LAT images were first processed in ilastik (55), a machine learning program for bio-image analysis, and then LAT pixel probabilities generated by ilastik were tracked in TrackMate. Analysis of NFAT localization was conducted semi-automatically using ilastik.

RESULTS

Fab'-DNA constructs are monovalent when conjugated to supported membranes

Fab'-DNA constructs were synthesized by digesting three commercially available anti-murine TCR antibodies: H57-597; 145-2C11; and 17A2, purifying the monovalent Fab' fragments, and conjugating those fragments to DNA oligonucleotides labeled with a single Atto647N dye, as described previously (see Materials and Methods for details) (Fig. S1 and S2 in the Supporting Material) (25).

Supported lipid bilayers (95% DOPC, 3% MCC-DOPE, and 2% Ni-NTA-DOGS phospholipids) were formed in imaging chambers and functionalized with a thiol-modified DNA oligonucleotide

(thiol-DNA) to which the Fab'-DNA molecules could hybridize. SLBs were first formed directly from unmodified SUVs followed by addition of the thiol-DNA, which became covalently linked to the MCC-DOPE lipids. The height of the Fab'-DNA above the bilayer was controlled by the length of this thiol-DNA strand. The shortest thiol-DNA strand was 16 nucleotides and precisely complemented the Fab' strand. Longer thiol-DNA strands were created by adding a 19 nt and 59 nt poly-T tail to the SLB-proximal 5' end (Fig 1c) (56). The length of the thiol-DNA strands were designed to allow for up to 14 nm, 25 nm, or 50 nm of vertical space between the SLB and the T cell plasma membrane at binding events between Fab'-DNA and TCR (Fig. S3). The shortest Fab'-DNA construct approximates the ~14 nm intermembrane space at pMHC:TCR binding events, excluding molecules with large extracellular domains, such as the phosphatase CD45, from close proximity to the binding event (21, 29, 41, 47). The longer constructs allow for intermembrane spacing at binding events that exceeds the height of CD45 extracellular domains (21-40 nm).

The SLB was then functionalized with Fab'-DNA and the adhesion molecule ICAM-1, which binds the integrin receptor LFA-1 and is critical to forming a continuous contact between T cells and antigen presenting cells. First the SLB was charged with Ni^{2+} to ensure stable chelation of polyhistidine-tagged ICAM-1 to the Ni-NTA DOGS lipids, and then Fab'-DNA and ICAM-1 were mixed and incubated in the imaging chamber for 35 min. Fab'-DNA rapidly anneals to the complementary thiol-DNA (Fig. 2a) and ICAM-1 couples to Ni-NTA lipids through multivalent interactions between Ni^{2+} and its histidine tag (51,65). Though the Atto647N dye used to label Fab'-DNA has a high membrane interaction factor (57), it has previously been confirmed that Fab'-DNA does not interact with the SLB in the absence of the thiol-DNA (25).

H57, 2C11, and 17A2 Fab'-DNA constructs were confirmed to be monovalently conjugated to the SLB using single molecule total internal reflection fluorescence (TIRF) microscopy. For

measurement of freely diffusing Fab'-DNA, images were taken with short exposure time (20 ms), high power (8.6 mW). In streaming image acquisitions (Movies S1 and S2), particles of uniform brightness diffuse across the SLB with uniform two-dimensional Brownian motion (Fig. 2b) and bleach in a single step (Fig. 2c). The FIJI plugin TrackMate was used to link images of single fluorophores into trajectories of diffusing particles, and the step size distribution of the resulting tracks were analyzed to obtain the diffusion coefficient of each Fab'-DNA construct. The step size distributions for both 2C11 Fab'-DNA and 17A2 Fab'-DNA, constructed using a multiple delay time protocol (see Supplemental Materials and Methods), were each well-fit by a single species Brownian diffusion model (Fig. 2d, 2f, Fig. S4):

$$\rho(r,\tau;D) = \frac{r}{2D\tau}\exp\left(\frac{-r^2}{4D\tau}\right), \qquad (1)$$

with molecular displacement, r, corresponding delay time, τ, and diffusion coefficient, D. D values for 2C11 Fab'-DNA and 17A2 Fab'-DNA were measured to be 2.49 ± 0.02 $\mu m^2/s$ and 2.83 ± 0.02 $\mu m^2/s$, respectively, in close agreement with the previously reported value of D = 2.43 ± 0.02 $\mu m^2/s$ for H57 Fab'-DNA on comparable supported bilayers (25). Step photobleaching analysis further confirmed that all Fab'-DNA ligands conjugated to the SLB as monomers. For both 2C11 and 17A2 Fab'-DNA constructs >99% of fluorescent signals bleached in a single step (Figs. 2e,g). The diffusion and step photobleaching data together provide strong evidence that Fab'-DNA exists on the supported membrane as a monovalent, monomeric ligand.

Single particle fluorescence intensity distributions of Fab'-DNA-Atto647N annealed to short (16 nt), medium (36 nt), and long (76 nt) thiol-DNA tethers confirm that the longer tethers create more space between Fab'-DNA and the SLB. In TIRF, illumination intensity decays exponentially from the interface (in this case, between glass and the water layer below the

bilayer), and so particle intensity can be a ruler for height for fluorophores in a uniform chemical environment. In this system, the Atto647N dye on Fab'-DNA annealed to the shortest thiol-DNA tether likely intercalates into the membrane, increasing the brightness of the fluorophore and slowing diffusion (25). The intensity distributions of Fab'-DNA-Atto647N annealed to the longer tethers are substantially dimmer, likely in part due to not interacting directly with the SLB and in part due to lower illumination intensity at increased height, and reflect the relative poly-T linker lengths (Fig. 2h). These data agree with the model of the poly-T linker as a worm-like chain with a persistence length of 1.5 – 3 nm in 150 mM salt and a fluorophore that can occupy a range of heights above the SLB (58). For systems where a labeled molecule lies flat on the membrane, this appears in the fluorescence signature (59). The medium and long thiol-DNA tethers are almost certainly not fully extended when diffusing freely on the bilayer, but they have the capability to extend up to 25 nm and 50 nm, respectively, in response to forces from the apposing T cell membrane.

All Fab' ligands bind TCR with high affinity

We then evaluated the interaction between T cells and SLB-tethered agonists by live-cell imaging of primary murine $CD4^+$ effector T cells expressing the AND TCR (details in Materials and Methods). T cells were added to imaging chambers containing a continuous SLB decorated with Fab'-DNA and ICAM-1 as described above that was equilibrated on the microscope to 37 °C. T cells made initial contact with the bilayer through interactions of adhesion receptor LFA-1 with ICAM-1, and then spread on the bilayer, creating a junction within which Fab'-DNA molecules could bind TCR (Fig. 3a). This junction was visualized using reflection interference contract microscopy (RICM). When Fab'-DNA binds TCR, its mobility dramatically decreases (Fig. 3b), as has been reported previously with other TCR ligands (15, 19, 60). Bound ligands are specifically resolved using a long, 500 ms exposure time, which allows slow-moving bound

Fab'-DNA to be clearly resolved while blurring the fluorescent signal from quickly diffusing unbound Fab'-DNA (Fig. 3c) (15). Bound Fab'-DNA was tracked through time, with 10 s time lapse between images to minimize photobleaching, enabling directly visualization of individual Fab'-DNA:TCR dwell times (Fig. 3a,d), and dwell time distributions for each ligand were assembled from those tracks (Fig. 3e). These distributions were fit with a single exponential decay, based on the first order dissociation kinetics of unbinding. After correcting for photobleaching, all Fab' ligands exhibited a dwell time, τ_{off}, of at least two minutes. In our experiments, Fab' ligands become difficult to track accurately after about two minutes due to the shuttling of bound TCR to the geometric center of the cell (Fig. 3a), and so these measured dwell times reflect a lower bound. Fab fragments are known to bind strongly to their binding partner, with the H57 Fab fragment reported to bind TCR stably for > 50 min (61). In contrast, the strong agonist MCC pMHC binds AND TCR with a reliably measured dwell time of about 50 sec using this method (15, 19, 20, 25).

The Fab'-DNA ligands in this study also bind TCR with a fast on-rate, corresponding to an overall very high efficiency of binding. The total number of Fab'-DNA ligands underneath a cell and the number of TCR-bound Fab'-DNA ligands can be independently measured to determine the fraction of bound Fab'-ligands at any point in time. All Fab' ligands can be resolved by rapidly acquiring short (50 ms) exposure images while bound Fab'-DNA:TCR complexes can be distinguished using long (500 ms) exposure images, in which the free ligands are diffusing too rapidly to produced well-defined images (Fig. 3f) (19, 25). The cell footprint on the bilayer is determined by RICM, and the fraction of ligands under the cell that are bound, a measure of the efficiency of ligand:receptor binding, can then be directly calculated. The median fraction bound was above 0.85 for all Fab'-DNA constructs, indicating that they all bind AND TCR very

efficiently (Fig. 3g). By comparison, about 30% of the strong agonist MCC pMHC, is observed bound to AND TCR at similar ligand densities (19).

We considered the possibility that Fab'-DNA constructs with longer tethers may have slower kinetic on rates due to their increased conformational degrees of freedom and therefore could have a lower measured fraction bound. This, however, was not the case; the measured fraction bound for H57 Fab'-DNA with the medium length (36 nt) and long (76 nt) DNA tethers were almost identical to the fraction of bound H57 Fab'-DNA with the short (16 nt) tether (Fig. S5).

Fab'-DNA potency is independent of binding epitope, but varies with DNA tether length

We characterize Fab'-DNA potency by measuring T cell activation vs. ligand density dose-response curves. Nuclear localization of the transcription factor nuclear factor for the activation of T cells (NFAT) is an indicator of early T cell activation and gives a clear binary readout of the T cell activation state (19, 20, 25). An NFAT localization reporter, lacking the DNA binding domain and fluorescently tagged with mCherry, allows for facile visualization of NFAT localization without modulating transcriptional activity (62). T cells transduced with the NFAT reporter were added to SLBs presenting ICAM-1 and Fab'-DNA or the strong pMHC agonist, MCC MHC. Cells were visualized landing and spreading on the bilayer, binding Fab'-DNA, and within minutes, translocating NFAT from the cytosol to the nucleus (Fig. 4a). Cells were defined as activated if the fluorescence intensity from the NFAT reporter was greater in the nucleus than in the cytosol (ratio > 1) (Fig. 4b). The potency of each ligand was measured by counting the fraction of activated cells 20 min after adding cells to bilayers with precisely quantified ligand density (Fig. S6a). Regardless of ligand binding epitope, all ligands that allowed about 14 nm spacing between the SLB and T cell plasma membrane at binding events, MCC pMHC and all Fab'-DNA constructs with 16 nt DNA tether, reached a half-maximal response at a ligand density of 0.2 – 0.4 μm^{-2} (Fig. 4c). By contrast, ligand potency was strongly influenced by the

length of the thiol-DNA tether. Ligands with DNA tethers that allowed about 25 nm and 50 nm of space between the SLB and T cell plasma membrane were 10 times and 100 times weaker, respectively, than the ligands that allowed an intermembrane space of about 14 nm (Fig. 4d, Fig. S6b).

Increased tether length decreases the efficiency of LAT activation by bound TCR

We finally investigate whether the low potency of Fab'-DNA constructs with longer tethers is rooted in their inability to trigger TCR efficiently despite their similarly robust binding or if it is due to a global negative cellular response. To do this, we probe phosphorylation activity downstream of the TCR. LAT forms a condensed assembly following phosphorylation by activated ZAP-70 kinases that are docked on triggered TCR (42, 45). These LAT condensates have recently been shown to occur even in response to single ligation events between agonist pMHC and TCR (44). Here, LAT clustering serves as a measure of proximal signaling from individual ligand:TCR binding events. T cells expressing LAT-eGFP were introduced to fluid supported lipid bilayers decorated with ICAM-1 and either a Fab'-DNA construct or the agonist MCC pMHC. Using multichannel TIRF microscopy, binding events were imaged as described above, using a long exposure time at low power to specifically image slowly moving ligand, and LAT-eGFP was imaged using low power and moderate exposure time to best capture the dynamic range of LAT fluorescent intensity in the cell being imaged. Cells were imaged starting upon initial contact with the bilayer and continuing for 120 s, during which LAT clustering in response to binding is most active, with a 2 s time lapse between successive frames. The density of Fab'-DNA on bilayers was kept very low (0.01-0.03 μm^{-2}) in order to best track single ligation events through time and capture the LAT clustering response to these events.

Snapshots from time sequences show clearly resolved binding events between ligand and TCR and concurrent local increase in LAT density at these binding events for potent ligands (Fig. 5a,

first four columns). Less potent ligands – those with longer DNA tethers that allowed for greater intermembrane space – experienced fewer LAT clusters colocalized binding events (Fig. 5a, last two columns). For potent ligands, a single binding event was sufficient to trigger significant LAT clustering (Fig. 3b, circled binding event; Fig. S7a), as has been previously reported for strong pMHC agonists (44). Moreover, T cells form LAT clusters in response to both Fab'-DNA and MCC pMHC when both ligands are presented on the bilayer at low density, indicating that T cells do not readily distinguish ligand identity and that the effects from multiple agonists are additive (Fig. S7b). Interestingly, instances where LAT clusters formed on bilayers presenting weak ligands with long DNA tethers often colocalized with clusters of binding events (Fig. S7c).

To quantify the signaling efficiency of each ligand, the total number of binding events experienced by a cell and the total number of LAT clusters formed within the cell were counted for first two minutes of the cell interacting with the supported membrane. Binding event trajectories were counted after tracking all events in TrackMate (54). LAT clusters were first identified in each frame using ilastik (55), a user-friendly machine learning algorithm for bio-image analysis, and then LAT pixel probability maps produced by ilastik were tracked in TrackMate (details in Materials and Methods). LAT clusters that persisted for at least 4 frames were counted in the analysis. The ratio of the number of LAT clusters to the number binding events was then calculated for each cell (Fig. 5c). Some LAT clusters form in the absence of binding (see ICAM only example in Fig. 5a), and so these ratios occasionally exceed one. In agreement with the NFAT titrations, all ligands that allowed about 14 nm spacing between the SLB and T cell plasma membrane produced LAT clusters with a similar efficiency per binding events, with medians of around 0.6. The ratio of LAT clusters to binding events significantly decreased with increasing intermembrane space (Fig. 5c). These results indicate that the difference in ligand potency seen at the level of transcription factor localization results from differences in the ligands' abilities to trigger TCR.

DISCUSSION

Implications for further Fab'-DNA development

Fab'-DNA shows promise as a tool to activate of polyclonal T cell populations in a manner similar to agonist pMHC; Fab'-DNA is monovalent and activates T cells at low ligand densities when membrane-associated but is inactive from solution (25). Here, we use the modular design of Fab'-DNA to test the dependence of T cell response on Fab'-DNA binding epitope and tether length. To achieve the goal of designing a universal TCR agonist, Fab's used in Fab'-DNA constructs must bind the constant region of the TCR, which is far from the pMHC binding site at the apex of the TCR variable region (Fig. 1b). The robust result that signaling from the TCR is indifferent to binding site allows flexibility in Fab' choice when using anti-murine Fab'-DNA and in designing Fab'-DNA constructs capable of binding and activating human T cells or perhaps chimeric antigen receptor T cells. That signaling potency depends on the spacing between apposed membranes at binding events is consistent with previous work with pMHC and therapeutic TCR-binding molecules (36, 48, 63, 64).

Relating results to proposed mechanisms of T cell antigen discrimination

The data presented in this study most closely relate to two proposed (and by no means mutually exclusive) mechanisms of T cell antigen discrimination: (1) kinetic-segregation and (2) anisotropic mechanosensing by the TCR. The kinetic-segregation model proposes that when TCR is localized in close contact zones between apposed membranes for a sufficient length of time, whether by ligand binding or not, the bulky and abundant phosphatase CD45 is excluded from the proximity of TCR (28–30, 40, 47, 65). CD45 exclusion increases the probability that TCR and proximal downstream kinases and scaffolding molecules are phosphorylated and leads to signal trandsuction (66). All results presented herein are consistent with kinetic-segregation. Interpreting the data according to this model, short Fab'-DNA ligands are able to

pin TCR in close contact zones that exclude CD45 for extended lengths of time, even if that zone is created by only a single binding event. Increasing the DNA tether length prevents the formation of close contact zones at binding events and increases the availability of bound TCR to CD45.

The relation of these data to the mechanosensing model is more complex. The model of the TCR as an anisotropic mechanosensor proposes that ligands able to exert a certain torque on the TCR are more effective at triggering TCR than ligands incapable of applying such torque. According to this model, force from pMHC binding is transmitted through the FG loop of TCRβ, causes allosteric change in the TCR/CD3 constant regions, and brings TCR/CD3 to a signaling-competent state (27, 67). H57 binds the FG loop of TCRβ, and is thought to trigger TCR by directly acting on this hinge when its Fab fragment is bound to a surface (32). 2C11 has two potential binding sites on the TCR/CD3 complex, as each complex has two CD3ε subunits. One CD3ε subunit sits directly above the FG loop, and 2C11 binding to this subunit has been proposed to act on the FG loop hinge similarly to H57 (26). The second CD3ε subunit sits approximately 120° away from the first (68). The observation that 2C11 Fab'-DNA has a similar potency as H57 Fab'-DNA and MCC pMHC suggests that 2C11 Fab'-DNA is able to trigger TCR regardless of which CD3ε subunit it binds. This interpretation is corroborated by 2C11 Fab'-DNA:TCR binding events producing LAT clusters with the same efficiency as H57 Fab'-DNA and MCC pMHC.

The results from 17A2 Fab'-DNA, matching results from all ligands that bind other epitopes, further underscore that TCR/CD3 appears to be indifferent to where it is bound. 17A2 binds the CD3ε/CD3γ cleft, off-axis from the FG loop fulcrum (26, 68). In experiments by Kim and coworkers, using optical tweezers and in the absence of adhesion, 17A2 antibody activated T cells only with the exertion of a tangential force. However in the experimental data we present

here is garnered from supported lipid bilayer assays with low 17A2 Fab'-DNA ligand density and in the context of physiologically dense ICAM-1:LFA-1 adhesion. In this configuration, Fab'-DNA;TCR binding always occurs within a few tens of nanometers of ICAM-1:LFA-1 adhesion complexes, and is not mechanically isolated from these (69, 70), apparently changing any directionality requirements. Notably, free lateral diffusion of ligands in the SLB prevents sustained tangential forces, and normal force applied to a single half antibody at a T cell–bead interface has been shown to be suffienct to activate T cells (71). It does not appear that TCR/CD3 is sensitive to which region or regions of the complex bear the load of a normal force in context of ICAM-1:LFA-1 adhesion.

More broadly interpreted, however, the results we present here still implicate force as an important mediator of TCR triggering by Fab'-DNA. TCRs bound the Fab'-DNA with short DNA tethers are more likely to sustain normal forces, due to the presence of larger ICAM-1:LFA-1 binding interactions and proteins on the T cell with large extracellular domains like CD45, compared to TCRs bound by Fab'-DNA with longer tethers.

Binding of a single Fab'-DNA is capable of creating significant TCR-proximal signaling

Our experiments are designed for facile, direct observation of single binding events between ligand and TCR with the ability to simultaneously image signaling response. With this design, we routinely see LAT condensates triggered by single ligand:TCR binding events with both pMHC (44) and Fab'-DNA ligands. These data stand in apparent contrast to a recently published, and carefully executed, study by Sevscik and coworkers that concludes that a similar monovalent H57-derived ligand, reported to allow 12-19 nm space between the SLB and T cell, activates T cells as efficiently as MCC pMHC only if two ligands are within a lateral distance of 20 nm from each other (72). Interestingly, in our study, the weaker Fab'-DNA ligands with longer DNA tethers were measured to be more likely to generate a LAT condensate if multiple ligands

are bound in a diffraction-limited area. This observation, that less potent ligands cause TCR-proximal signaling more readily when they are clustered, may relate to other studies that report ligand clustering as a requirement for signaling using similar experimental platforms (60, 72).

In conclusion, through modulating the binding epitope and DNA tether length of Fab'-DNA constructs, we find that varying the DNA tether length affects Fab'-DNA potency, but varying the binding epitope does not. These findings advance the utility of membrane-linked Fab'-DNA ligands as universal T cell agonists and clarify design criteria for further development of this class of synthetic T call activators.

Acknowledgements

We are grateful to members of the Groves Laboratory for critical feedback on this manuscript. We thank F. Marangoni (Harvard Medical School) for providing the NFAT reporter plasmid. We thank L. Teyton (Scripps Research Institute) and M. Davis (Stanford University) for providing the MHC and ICAM-1 bacmids. We thank Scott Hansen (University of Oregon) for cloning the NFATmCherry-P2A-LAT-eGFP construct.

The financial support for this work was provided by National Institutes of Health grant P01 AI091580 and by the Novo Nordisk Foundation Challenge Programme as part of the Center for Geometrically Engineered Cellular Systems.

Author Contributions

JTG and KBW conceived and designed this study. KBW and SM performed experiments. KBW, SM and DMB contributed new reagents/analytical tools. KBW, SM, SK, MKO'D, and DMB harvested and prepared T cells for experiments. KBW analyzed data. KBW and JTG wrote the manuscript. All authors edited the manuscript.

Competing interests

The authors declare that they have no competing interests.

REFERENCES

1. Weiss, A., J. Imboden, K. Hardy, B. Manger, C. Terhorst, and J. Stobo. 1986. The Role of the T3/Antigen Receptor Complex in T-Cell Activation. *Annu. Rev. Immunol.* 4:593–619.
2. Kaye, J., S. Porcelli, J. Tite, B. Jones, and C.A. Janeway. 1983. Both a monoclonal antibody and antisera specific for determinants unique to individual cloned helper T cell lines can substitute for antigen and antigen-presenting cells in the activation of T cells. *J. Exp. Med.* 158:836–856.
3. Kubo, R.T., W. Born, J.W. Kappler, P. Marrack, and M. Pigeon. 1989. Characterization of a monoclonal antibody which detects all murine alpha beta T cell receptors. *J. Immunol.* 142:2736–42.
4. Leo, O., M. Foo, D.H. Sachs, L.E. Samelson, and J.A. Bluestone. 1987. Identification of a monoclonal antibody specific for a murine T3 polypeptide. *Proc. Natl. Acad. Sci. U. S. A.* 84:1374–1378.
5. Miescher, G.C., M. Schreyer, and H.R. MacDonald. 1989. Production and characterization of a rat monoclonal antibody against the murine CD3 molecular complex. *Immunol. Lett.* 23:113–118.
6. Irving, B.A., and A. Weiss. 1991. The cytoplasmic domain of the T cell receptor ζ chain is sufficient to couple to receptor-associated signal transduction pathways. *Cell*. 64:891–901.
7. Boniface, J.J., J.D. Rabinowtiz, C. Wulfing, J. Hampi, Z. Reich, J.D. Altman, R.M. Kantor, C. Beeson, H.M. McConnell, and M.M. Davis. 1998. Erratum: Initiation of signal transduction through the T cell receptor requires the multivalent engagement of peptide/MHC ligands (Immunity 9 (459- 466)). *Immunity*. 9:891.
8. Kaye, J., and C.A. Janeway. 1984. The Fab fragment of a directly activating monoclonal antibody that precipitates a disulfide-linked heterodimer from a helper T cell clone blocks activation by either allogeneic Ia or antigen and self-Ia. *J. Exp. Med.* 159:1397–1412.
9. Altman, J.D., P.A.H. Moss, P.J.R. Goulder, D.H. Barouch, M.G. McHeyzer-Williams, J.I. Bell, A.J. McMichael, and M.M. Davis. 1996. Phenotypic analysis of antigen-specific T lymphocytes. *Science (80-.).* 274:94–96.
10. Johnson, K.G., S.K. Bromley, M.L. Dustin, and M.L. Thomas. 2000. A supramolecular basis for CD45 tyrosine phosphatase regulation in sustained T cell activation. *Proc. Natl. Acad. Sci.* 97:10138–10143.
11. Ledbetter, J.A., C.H. June, L.S. Grosmaire, and P.S. Rabinovitch. 1987. Crosslinking of surface antigens causes mobilization of intracellular ionized calcium in T lymphocytes. *Proc. Natl. Acad. Sci.* 84:1384–1388.
12. Irvine, D.J., M.A. Purbhoo, M. Krogsgaard, and M.M. Davis. 2002. Direct observation of ligand recognition by T cells. *Nature*. 419:845–849.
13. Purbhoo, M.A., D.J. Irvine, J.B. Huppa, and M.M. Davis. 2004. T cell killing does not require the formation of a stable mature immunological synapse. *Nat. Immunol.* 5:524–530.
14. Huang, J., M. Brameshuber, X. Zeng, J. Xie, Q. jing Li, Y. hsiu Chien, S. Valitutti, and M.M. Davis. 2013. A Single peptide-major histocompatibility complex ligand triggers digital cytokine secretion in CD4+ T Cells. *Immunity*. 39:846–857.
15. O ’Donoghue, G.P., R.M. Pielak, A.A. Smoligovets, J.J. Lin, and J.T. Groves. 2013. Direct

single molecule measurement of TCR triggering by agonist pMHC in living primary T cells. *Elife*. 2.
16. Demotz, S., H.M. Grey, and A. Sette. 1990. The Minimal Number of Class II MHC-Antigen Complexes Needed for T Cell Activation. *Science (80-.).* 249:1028–1030.
17. Harding, C. V., and E.R. Unanue. 1990. Quantitation of antigen-presenting cell MHC class II/peptide complexes necessary for T-cell stimulation. *Nature*. 346:574–576.
18. Bozzacco, L., H. Yu, H.A. Zebroski, J. Dengjel, H. Deng, S. Mojsov, and R.M. Steinman. 2011. Mass spectrometry analysis and quantitation of peptides presented on the MHC II molecules of mouse spleen dendritic cells. *J. Proteome Res.* 10:5016–5030.
19. Pielak, R.M., G.P. O'Donoghue, J.J. Lin, K.N. Alfieri, N.C. Fay, S.T. Low-Nam, and J.T. Groves. 2017. Early T cell receptor signals globally modulate ligand: receptor affinities during antigen discrimination. *Proc. Natl. Acad. Sci. U. S. A.* 114:12190–12195.
20. Lin, J.J.Y., S.T. Low-Nam, K.N. Alfieri, D.B. McAffee, N.C. Fay, and J.T. Groves. 2019. Mapping the stochastic sequence of individual ligand-receptor binding events to cellular activation: T cells act on the rare events. *Sci. Signal.* 12:1–14.
21. Varma, R., G. Campi, T. Yokosuka, T. Saito, and M.L. Dustin. 2006. T Cell Receptor-Proximal Signals Are Sustained in Peripheral Microclusters and Terminated in the Central Supramolecular Activation Cluster. *Immunity*. 25:117–127.
22. Mossman, K.D., G. Campi, J.T. Groves, and M.L. Dustin. 2005. Altered TCR Signaling from Geometrically Repatterned Immunological Synapses. *Science (80-.).* 310:1191–1193.
23. Monks, C.R.F., B.A. Freiberg, H. Kupfer, N. Sciaky, and A. Kupfer. 1998. Three-dimensional segregation of supramolecular activation clusters in T cells. *Nature*. 395:82–86.
24. Grakoui, A., S.K. Bromley, C. Sumen, M.M. Davis, A.S. Shaw, P.M. Allen, and M.L. Dustin. 1999. The immunological synapse: A molecular machine controlling T cell activation. *Science (80-.).* 285:221–227.
25. Lin, J.J., G.P. O'Donoghue, K.B. Wilhelm, M.P. Coyle, S.T. Low-Nam, N.C. Fay, K.N. Alfieri, and J.T. Groves. 2020. Membrane Association Transforms an Inert Anti-TCRβ Fab' Ligand into a Potent T Cell Receptor Agonist. *Biophys. J.* 118:2879–2893.
26. Kim, S.T., K. Takeuchi, Z.Y.J. Sun, M. Touma, C.E. Castro, A. Fahmy, M.J. Lang, G. Wagner, and E.L. Reinherz. 2009. The αβ T cell receptor is an anisotropic mechanosensor. *J. Biol. Chem.*
27. Brazin, K.N., R.J. Mallis, D.K. Das, Y. Feng, W. Hwang, J. huai Wang, G. Wagner, M.J. Lang, and E.L. Reinherz. 2015. Structural features of the aβTCR mechanotransduction apparatus that promote pMHC discrimination. *Front. Immunol.* 6.
28. Davis, S.J., and P.A. van der Merwe. 2006. The kinetic-segregation model: TCR triggering and beyond. *Nat. Immunol.* 7:803–809.
29. James, J.R., and R.D. Vale. 2012. Biophysical mechanism of T-cell receptor triggering in a reconstituted system. *Nature*. 487:64–69.
30. Chang, V.T., R.A. Fernandes, K.A. Ganzinger, S.F. Lee, C. Siebold, J. McColl, P. Jönsson, M. Palayret, K. Harlos, C.H. Coles, E.Y. Jones, Y. Lui, E. Huang, R.J.C. Gilbert, D. Klenerman, A.R. Aricescu, and S.J. Davis. 2016. Initiation of T cell signaling by CD45 segregation at "close contacts." *Nat. Immunol.* 17:574–582.
31. Wang, J.H., K. Lim, A. Smolyar, M.K. Teng, J.H. Liu, A.G.D. Tse, J. Liu, R.E. Hussey, Y. Chishti, C.T. Thomson, R.M. Sweet, S.G. Nathenson, H.C. Chang, J.C. Sacchettini, and E.L. Reinherz. 1998. Atomic structure of an αβ T cell receptor (TCR) heterodimer in complex with an anti-TCR Fab fragment derived from a mitogenic antibody. *EMBO J.* 17:10–26.
32. Das, D.K., Y. Feng, R.J. Mallis, X. Li, D.B. Keskin, R.E. Hussey, S.K. Brady, J.H. Wang, G. Wagner, E.L. Reinherz, and M.J. Lang. 2015. Force-dependent transition in the T-cell

receptor β-subunit allosterically regulates peptide discrimination and pMHC bond lifetime. *Proc. Natl. Acad. Sci. U. S. A.* 112:1517–1522.
33. Hwang, W., R.J. Mallis, M.J. Lang, and E.L. Reinherz. 2020. The αβTCR mechanosensor exploits dynamic ectodomain allostery to optimize its ligand recognition site. *Proc. Natl. Acad. Sci. U. S. A.* 117:21336–21345.
34. Garboczi, D.N., P. Ghosh, U. Utz, Q.R. Fan, W.E. Biddison, and D.C. Wiley. 1996. Structure of the complex between human T-cell receptor, viral peptide, and HLA-A2. *Nature*. 384:134–141.
35. Garcia, K.C., M. Degano, L.R. Pease, M. Huang, P.A. Peterson, L. Teyton, and I.A. Wilson. 1998. Structural Basis of Plasticity in T Cell Receptor Recognition of a Self Peptide-MHC Antigen. *Science (80-.).* 279:1166–1172.
36. Choudhuri, K., D. Wiseman, M.H. Brown, K. Gould, and P.A. Van Der Merwe. 2005. T-cell receptor triggering is critically dependent on the dimensions of its peptide-MHC ligand. *Nature*. 436:578–582.
37. Springer, T.A. 1990. Adhesion Receptors of the Immune System. *Nature*. 346:425–434.
38. Woollett, G.R., A.F. Williams, and D.M. Shotton. 1985. Visualisation by low-angle shadowing of the leucocyte-common antigen. A major cell surface glycoprotein of lymphocytes. *EMBO J.* 4:2827–2830.
39. McCall, M.N., D.M. Shotton, and A.N. Barclay. 1992. Expression of soluble isoforms of rat CD45. Analysis by electron microscopy and use in epitope mapping of anti-CD45R monoclonal antibodies. *Immunology*. 76:310–7.
40. Carbone, C.B., N. Kern, R.A. Fernandes, E. Hui, X. Su, K.C. Garcia, and R.D. Vale. 2017. In vitro reconstitution of T cell receptor-mediated segregation of the CD45 phosphatase. *Proc. Natl. Acad. Sci. U. S. A.* 114:E9338–E9345.
41. Van Der Merwe, P.A., and O. Dushek. 2011. Mechanisms for T cell receptor triggering. *Nat. Rev. Immunol.* 11:47–55.
42. Zhang, W., J. Sloan-Lancaster, J. Kitchen, R.P. Trible, and L.E. Samelson. 1998. LAT: The ZAP-70 tyrosine kinase substrate that links T cell receptor to cellular activation. *Cell*. 92:83–92.
43. Nag, A., M.I. Monine, J.R. Faeder, and B. Goldstein. 2009. Aggregation of Membrane Proteins by Cytosolic Cross-Linkers: Theory and Simulation of the LAT-Grb2-SOS1 System. *Biophys. J.* 96:2604–2623.
44. Ganti, R.S., W.-L. Lo, D.B. McAffee, J.T. Groves, A. Weiss, and A.K. Chakraborty. 2020. How the T cell signaling network processes information to discriminate between self and agonist ligands. *Proc. Natl. Acad. Sci.* 117:26020–26030.
45. Balagopalan, L., R.L. Kortum, N.P. Coussens, V.A. Barr, and L.E. Samelson. 2015. The Linker for Activation of T Cells (LAT) Signaling Hub: From Signaling Complexes to Microclusters. *J. Biol. Chem.* 290:26422–26429.
46. Wild, M.K., A. Cambiaggi, M.H. Brown, E.A. Davies, H. Ohno, T. Saito, and P.A. van der Merwe. 1999. Dependence of T Cell Antigen Recognition on the Dimensions of an Accessory Receptor–Ligand Complex. *J. Exp. Med.* 190:31–42.
47. Van Der Merwe, P.A., S.J. Davis, A.S. Shaw, and M.L. Dustin. 2000. Cytoskeletal polarization and redistribution of cell-surface molecules during T cell antigen recognition. *Semin. Immunol.* 12:5–21.
48. Bluemel, C., S. Hausmann, P. Fluhr, M. Sriskandarajah, W.B. Stallcup, P.A. Baeuerle, and P. Kufer. 2010. Epitope distance to the target cell membrane and antigen size determine the potency of T cell-mediated lysis by BiTE antibodies specific for a large melanoma surface antigen. *Cancer Immunol. Immunother.* 59:1197–1209.
49. Rangarajan, S., Y. He, Y. Chen, M.C. Kerzic, B. Ma, R. Gowthaman, B.G. Pierce, R. Nussinov, R.A. Mariuzza, and J. Orban. 2018. Peptide–MHC (pMHC) binding to a human antiviral T cell receptor induces long-range allosteric communication between pMHC- and

CD3-binding sites. *J. Biol. Chem.* 293:15991–16005.
50. Coyle, M.P., Q. Xu, S. Chiang, M.B. Francis, and J.T. Groves. 2013. DNA-mediated assembly of protein heterodimers on membrane surfaces. *J. Am. Chem. Soc.* 135:5012–5016.
51. Kaye, J., M.-L. Hsu, M.-E. Sauron, S.C. Jameson, N.R.J. Gascoigne, and S.M. Hedrick. 1989. Selective development of CD4+ T cells in transgenic mice expressing a class II MHC-restricted antigen receptor. *Nature*. 341:746–749.
52. Smith, A.W., A.A. Smoligovets, and J.T. Groves. 2011. Patterned Two-Photon Photoactivation Illuminates Spatial Reorganization in Live Cells. *J. Phys. Chem. A*. 115:3867–3875.
53. Edelstein, A., N. Amodaj, K. Hoover, R. Vale, and N. Stuurman. 2010. Computer Control of Microscopes Using µManager. *Curr. Protoc. Mol. Biol.* 92.
54. Tinevez, J.Y., N. Perry, J. Schindelin, G.M. Hoopes, G.D. Reynolds, E. Laplantine, S.Y. Bednarek, S.L. Shorte, and K.W. Eliceiri. 2017. TrackMate: An open and extensible platform for single-particle tracking. *Methods*. 115:80–90.
55. Berg, S., D. Kutra, T. Kroeger, C.N. Straehle, B.X. Kausler, C. Haubold, M. Schiegg, J. Ales, T. Beier, M. Rudy, K. Eren, J.I. Cervantes, B. Xu, F. Beuttenmueller, A. Wolny, C. Zhang, U. Koethe, F.A. Hamprecht, and A. Kreshuk. 2019. Ilastik: Interactive Machine Learning for (Bio)Image Analysis. *Nat. Methods*. 16:1226–1232.
56. Taylor, M.J., K. Husain, Z.J. Gartner, S. Mayor, and R.D. Vale. 2017. A DNA-Based T Cell Receptor Reveals a Role for Receptor Clustering in Ligand Discrimination. *Cell*. 169:108-119.e20.
57. Hughes, L.D., R.J. Rawle, and S.G. Boxer. 2014. Choose Your Label Wisely: Water-Soluble Fluorophores Often Interact with Lipid Bilayers. *PLoS One*. 9:e87649.
58. Murphy, M.C., I. Rasnik, W. Cheng, T.M. Lohman, and T. Ha. 2004. Probing Single-Stranded DNA Conformational Flexibility Using Fluorescence Spectroscopy. *Biophys. J.* 86:2530–2537.
59. Parthasarathy, R., D. Rabuka, C.R. Bertozzi, and J.T. Groves. 2007. Molecular orientation of membrane-anchored mucin glycoprotein mimics. *J. Phys. Chem. B*. 111:12133–12135.
60. Taylor, M.J., K. Husain, Z.J. Gartner, S. Mayor, and R.D. Vale. 2017. A DNA-Based T Cell Receptor Reveals a Role for Receptor Clustering in Ligand Discrimination. *Cell*. 169:108–119.
61. Huppa, J.B., M. Axmann, M.A. Mörtelmaier, B.F. Lillemeier, E.W. Newell, M. Brameshuber, L.O. Klein, G.J. Schütz, and M.M. Davis. 2010. TCR–peptide–MHC interactions in situ show accelerated kinetics and increased affinity. *Nature*. 463:963–967.
62. Marangoni, F., T.T. Murooka, T. Manzo, E.Y. Kim, E. Carrizosa, N.M. Elpek, and T.R. Mempel. 2013. The Transcription Factor NFAT Exhibits Signal Memory during Serial T Cell Interactions with Antigen-Presenting Cells. *Immunity*. 38:237–249.
63. Cai, H., J. Muller, D. Depoil, V. Mayya, M.P. Sheetz, M.L. Dustin, and S.J. Wind. 2018. Full control of ligand positioning reveals spatial thresholds for T cell receptor triggering. *Nat. Nanotechnol.* 13:610–617.
64. Chen, B.M., M.A. Al-Aghbar, C.H. Lee, T.C. Chang, Y.C. Su, Y.C. Li, S.E. Chang, C.C. Chen, T.H. Chung, Y.C. Liao, C.H. Lee, and S.R. Roffler. 2017. The affinity of elongated membrane-tethered ligands determines potency of T cell receptor triggering. *Front. Immunol.* 8:1–21.
65. Fernandes, R.A., K.A. Ganzinger, J.C. Tzou, P. Jönsson, S.F. Lee, M. Palayret, A.M. Santos, A.R. Carr, A. Ponjavic, V.T. Chang, C. Macleod, B. Christoffer Lagerholm, A.E. Lindsay, O. Dushek, A. Tilevik, S.J. Davis, and D. Klenerman. 2019. A cell topography-based mechanism for ligand discrimination by the T cell receptor. *Proc. Natl. Acad. Sci. U. S. A.* 116:14002–14010.

66. Hui, E., and R.D. Vale. 2014. In vitro membrane reconstitution of the T-cell receptor proximal signaling network. *Nat. Struct. Mol. Biol.* 21:133–142.
67. Reinherz, E.L. 2019. The structure of a T-cell mechanosensor. *Nature*. 7–9.
68. Dong, D., L. Zheng, J. Lin, B. Zhang, Y. Zhu, N. Li, S. Xie, Y. Wang, N. Gao, and Z. Huang. 2019. Structural basis of assembly of the human T cell receptor–CD3 complex. *Nature*. 573:546–552.
69. Qi, S.Y., J.T. Groves, and A.K. Chakraborty. 2001. Synaptic pattern formation during cellular recognition. *Proc. Natl. Acad. Sci.* 98:6548–6553.
70. Kaizuka, Y., and J.T. Groves. 2006. Hydrodynamic Damping of Membrane Thermal Fluctuations near Surfaces Imaged by Fluorescence Interference Microscopy. *Phys. Rev. Lett.* 96:118101.
71. Feng, Y., K.N. Brazin, E. Kobayashi, R.J. Mallis, E.L. Reinherz, and M.J. Lang. 2017. Mechanosensing drives acuity of *αβ* T-cell recognition. *Proc. Natl. Acad. Sci.*
72. Hellmeier, J., R. Platzer, A.S. Eklund, T. Schlichthaerle, A. Karner, V. Motsch, M.C. Schneider, E. Kurz, V. Bamieh, M. Brameshuber, J. Preiner, R. Jungmann, H. Stockinger, G.J. Schütz, J.B. Huppa, and E. Sevcsik. 2021. DNA origami demonstrate the unique stimulatory power of single pMHCs as T cell antigens. *Proc. Natl. Acad. Sci. U. S. A.* 118.

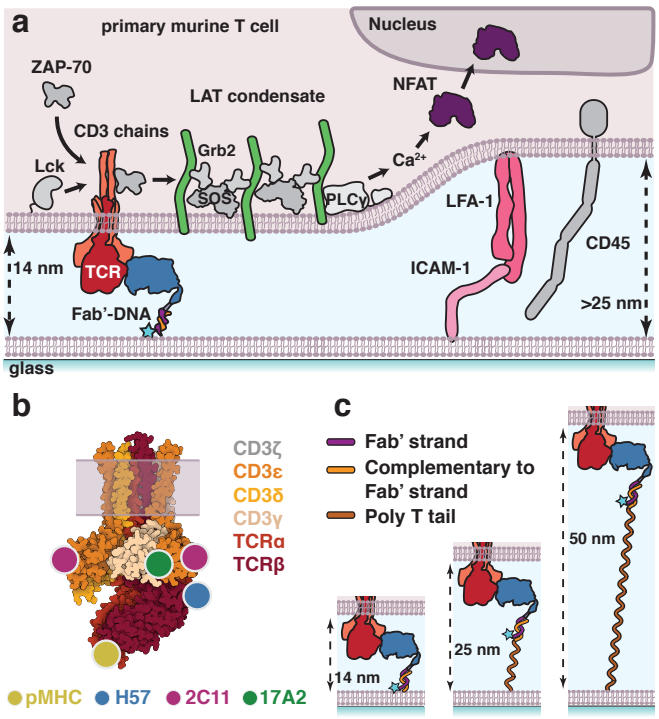
a
primary murine T cell
Nucleus
ZAP-70
LAT condensate
NFAT
CD3 chains
Grb2
Lck
Ca2+
SOS
PLCγ
LFA-1
CD45
14 nm
TCR
ICAM-1
>25 nm
Fab'-DNA
glass
b
CD3ζ
CD3ε
CD3δ
CD3γ
TCRα
TCRβ
pMHC
H57
2C11
17A2
c
Fab' strand
Complementary to Fab' strand
Poly T tail
14 nm
25 nm
50 nm

Figure 1. Fab'-DNA is a modular TCR ligand. (**A**) Fab'-DNA and ICAM-1 are presented on supported lipid bilayers. Upon adding T cells to the bilayer, LFA-1 adheres to ICAM-1 to create a stable intermembrane junction between the SLB and T cell. Within this junction, Fab'-DNA binds TCR, creating a narrow 14 nm space between membranes that excludes ICAM-1:LFA-1 conjugates and the phosphatase CD45 from close proximity. Productive TCR triggering is monitored by the formation of TCR-proximal LAT condensates and cellular activation is monitored by translocation of the transcription factor NFAT from the cytosol to the nucleus. (**B**) Fab'-DNA constructs are synthesized from antibodies that bind three distinct epitopes on the TCR/CD3 complex (PDB 6JXR). Binding epitopes for pMHC and all Fabs have previously been determined by crystal and NMR structures and are approximately mapped onto the TCR/CD3 cryoEM structure. (**C**) The spacing between the SLB and T cell at Fab'-DNA:TCR binding events is modulated by varying the length of the DNA tether. A poly-T tail is added to the membrane-proximal 5' end of the thiol-DNA, increasing the allowed distance between the membrane and the region of the thiol-DNA to which Fab'-DNA anneals.

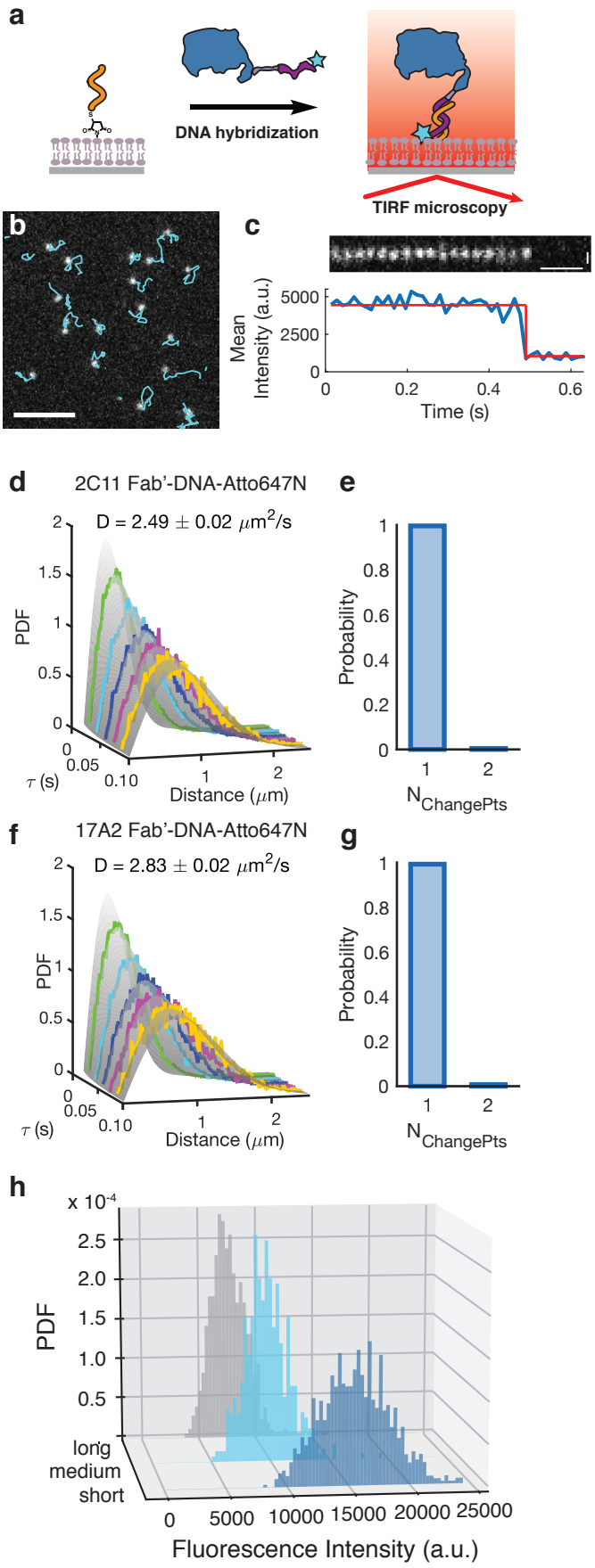
a
DNA hybridization
TIRF microscopy
b
c
Mean Intensity (a.u.)
5000
2500
0
0
0.2
0.4
0.6
Time (s)
d
2C11 Fab'-DNA-Atto647N
D = 2.49 ± 0.02 μm²/s
PDF
τ (s)
Distance (μm)
e
Probability
N ChangePts
f
17A2 Fab'-DNA-Atto647N
D = 2.83 ± 0.02 μm²/s
g
h
x 10⁻⁴
PDF
long
medium
short
0
5000
10000
15000
20000
25000
Fluorescence Intensity (a.u.)

Figure 2. All Fab'-DNA constructs diffuse as monomers on supported lipid bilayers. (**A**) The thiol-DNA strand is covalently bound to the SLB via thiol/maleimide chemistry. Fab'-DNA that is labeled with a single Atto647N fluorophore is then incubated in the imaging chambers and anneals to the thiol-DNA strand. Fab'-DNA molecules are visualized using TIRF microscopy. (**B**) 2C11 Fab'-DNA molecules of uniform brightness undergo Brownian diffusion on the SLB. Scale bar 5 μm. (**C**) Diffusing 2C11 Fab'-DNA particles bleach in a single step, confirming that each particle is a single Fab'-DNA molecule. Vertical scale bar 500 nm. Horizontal scale bar 0.1 s. (**D** and **F**) The step size distribution of 2C11 (D) and 17A2 (F) Fab'-DNA fits a single component diffusion model well. A multi-delay time protocol was used to build step size distributions at multiple time delays and all distributions were simultaneously fit to obtain the diffusion coefficient for each ligand. Error indicates the 95% CI. (n > 50,000 steps) Data are representative of three experiments. (**E** and **G**). >99% of 2C11 (n = 122) (E) and 17A2 (n = 175) (G) Fab'-DNA particles bleach in a single step. These data were obtained on gel-phase SLBs to enable tracking of particles for their full trajectories until photobleaching. The <1% of particles that undergo 2-step photobleaching match the probability that two Fab'-DNA are randomly spaced below the diffraction limit. No particles bleach in three or more steps. Panels B-G display data collected with the shortest thiol-DNA. (**H**) Single particle fluorescence intensity distributions for Fab'-DNA conjugated to the SLB by annealing to short, medium, and long thiol-DNA strands show decreased fluorescence intensity with increased tether length. Short thiol-DNA: n > 1000 particles; medium thiol-DNA: n > 500 particles; long thiol-DNA: n > 1000 particles.

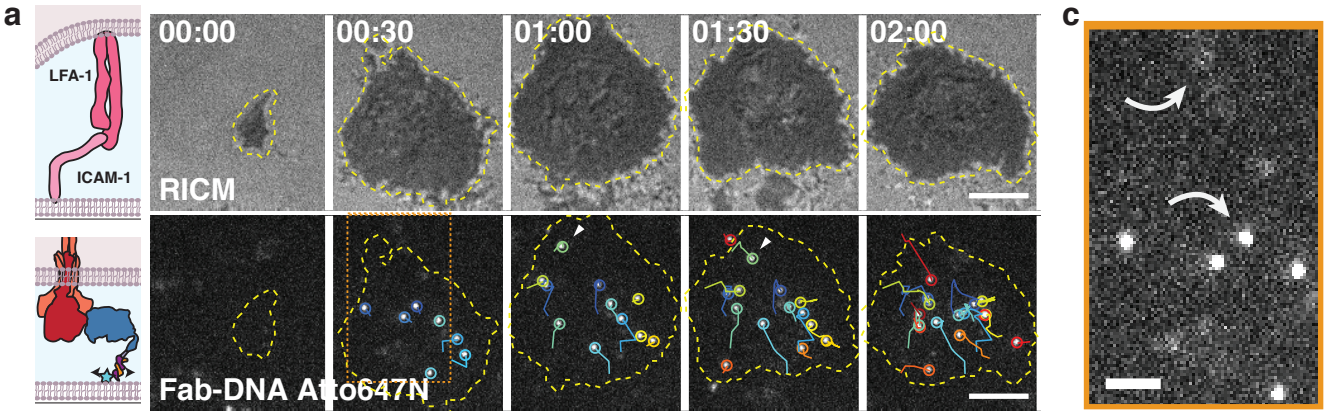

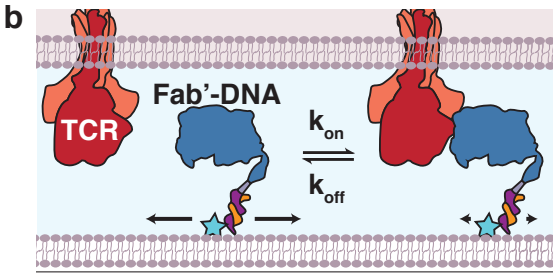

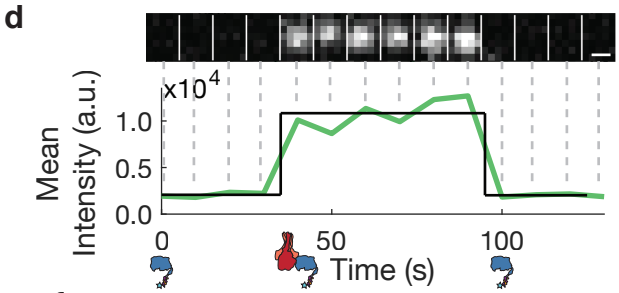

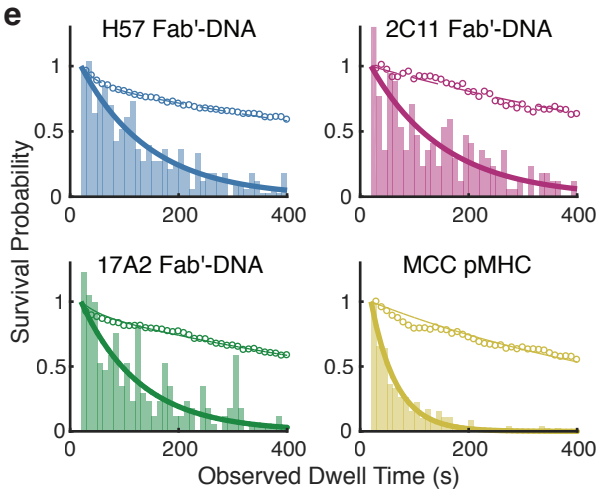

	τ_{obs}	τ_{bl}	τ_{off}	n
H57	129 ± 9	1000 ± 200	140 ± 20*	423
2C11	135 ± 18	800 ± 60	160 ± 30*	240
17A2	109 ± 13	900 ± 100	120 ± 20*	227
MCC pMHC	46 ± 2	690 ± 40	49 ± 3	366

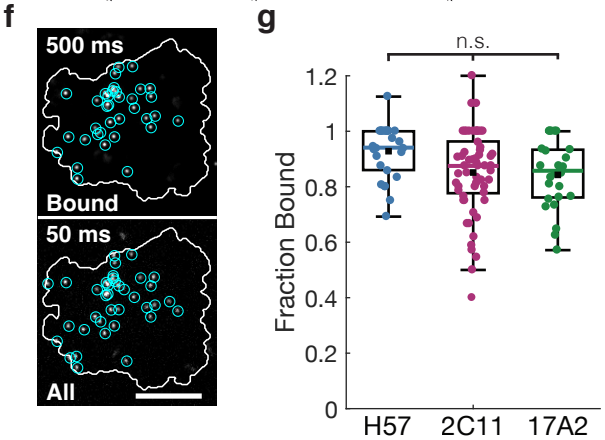

Figure 3. Measurements of individual binding events between Fab'-DNA and TCR illustrate that all Fab'-DNA complexes strongly bind TCR. (**A**) T cells adhere to the bilayer through ICAM-1:LFA-1 interactions (cell footprint visualized by RICM), and Fab'-DNA-Atto647N binds TCR within this SLB - T cell junction (visualized by TIRF). Each binding event is tracked through time, denoted with a unique color for each event. Scale bar 5 μm. (**B**) Bound Fab'-DNA is distinguished from unbound Fab'-DNA by the dramatic decrease in Fab'-DNA mobility upon TCR binding. (**C**) An imaging strategy using a long, 500 ms exposure time at low power allows slowly-moving bound Fab'-DNA images (bottom arrow) to be resolved while quickly diffusing free Fab'-DNA forms a blurred image (top arrow). This area corresponds to the area in (A) outlined by a dotted orange line. Scale bar 2 μm. (**D**) The intensity trace of a Fab'-DNA :TCR binding event through time (white arrow in (A)) illustrates that single binding and unbinding events are readily visualized. Scale bar 300 nm. (**E**) Dwell time distributions, corrected for photobleaching (empty circles), for Fab'-DNA ligands illustrate their very slow off-rates. Fab'-DNA ligands bind for at least twice as long as the strong agonist pMHC. *The reported τ_{off} for Fab'-DNA ligands are underestimates due to difficulty tracking ligands as they approach the center of the SLB - T cell junction. Data are from constructs with 14 nm intermembrane space. (**F**) Bound ligand and all ligand under a cell footprint are imaged with long and short exposure times, respectively. Scale bar 5 μm. (**G**) The fraction of Fab'-DNA ligands bound under T cells is very high all Fab'-DNA constructs. Colored bar: median; black square: mean; box: interquartile range; whiskers: data within 1.5x IQR. Significance was determined by the Mann-Whitney U test (n.s. $p > 0.01$) (H57: n = 27; 2C11: n = 58; 17A2: n = 26). Data are from constructs with 14 nm intermembrane space. Data are compiled from cells from at least two mice for each condition in dwell time and fraction bound measurements.

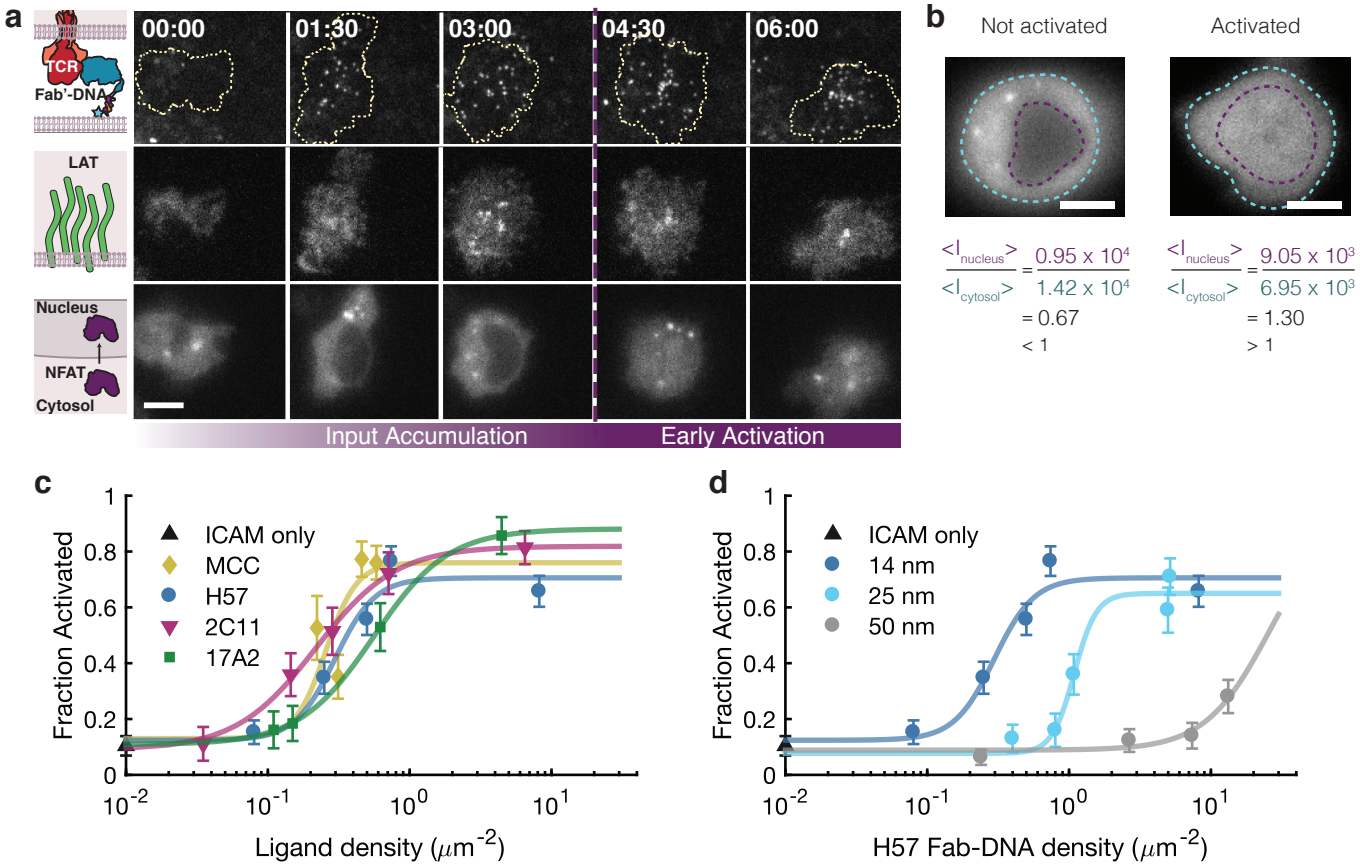
a
TCR
Fab'-DNA
LAT
Nucleus
NFAT
Cytosol
00:00
01:30
03:00
04:30
06:00
Input Accumulation
Early Activation
b
Not activated
Activated
$\frac{\langle I_{nucleus}\rangle}{\langle I_{cytosol}\rangle} = \frac{0.95 \times 10^4}{1.42 \times 10^4} = 0.67 < 1$
$\frac{\langle I_{nucleus}\rangle}{\langle I_{cytosol}\rangle} = \frac{9.05 \times 10^3}{6.95 \times 10^3} = 1.30 > 1$
c
Fraction Activated
ICAM only
MCC
H57
2C11
17A2
Ligand density (μm^{-2})
d
Fraction Activated
ICAM only
14 nm
25 nm
50 nm
H57 Fab-DNA density (μm^{-2})

Figure 4. T cells activate with similar probabilities regardless of ligand binding epitope, but have lower activation response when stimulated with Fab'-DNA ligands with longer tethers. (**A**) Cells added to supported lipid bilayers make adhesion contacts, bind TCR ligand (top row), respond to TCR triggering, visualized by LAT condensate formation (middle row), and may activate, visualized by NFAT reporter fluorescence intensity accumulating in the nucleus. Scale bar 5 μm. (**B**) Cells are defined as activated if the ratio of fluorescence intensity in the nucleus to the cytosol is greater than one and not activated if the ratio is less than one. Scale bar 5 μm. (**C** and **D**) Dose-response curves for each ligand are built by adding cells to bilayers with precisely quantified density of ligand, letting cells interact with the bilayers for 20 min, then determining the fraction of activated cells for each condition. n > 50 cells for all conditions. Error bars denote the SEM. Data are representative of at least two biological replicates. (**C**) All ligands that create close, ~14 nm intermembrane spaces at binding events activate with similar potency, regardless of ligand binding epitope. (**D**) H57 Fab'-DNA potency significantly decreases as the length of the DNA tether increases.

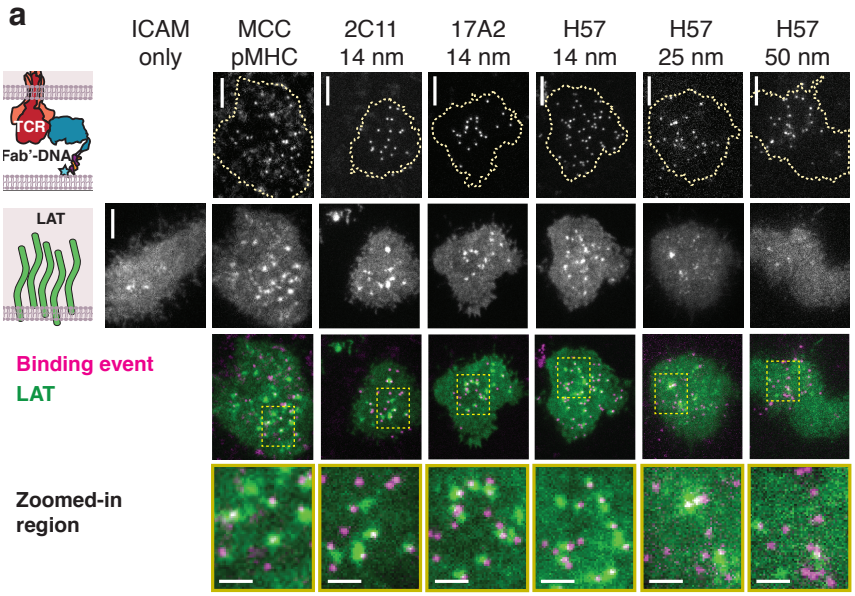
a
ICAM only
MCC pMHC
2C11 14 nm
17A2 14 nm
H57 14 nm
H57 25 nm
H57 50 nm
TCR
Fab'-DNA
LAT
Binding event
LAT
Zoomed-in region

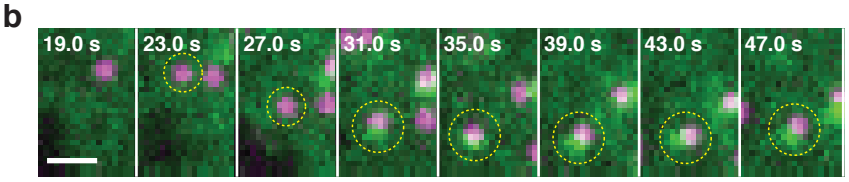
b
19.0 s
23.0 s
27.0 s
31.0 s
35.0 s
39.0 s
43.0 s
47.0 s

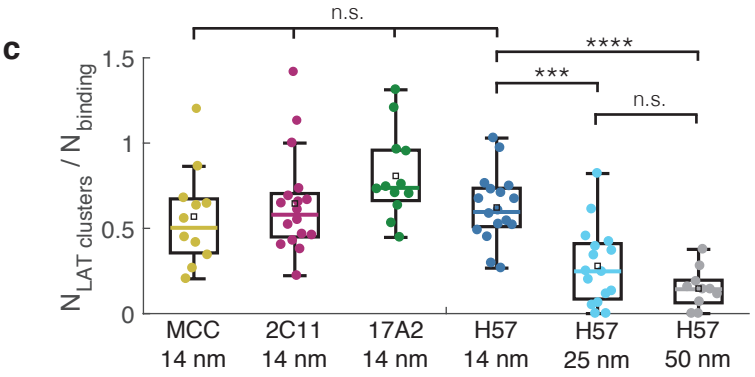
c
n.s.
****
***
n.s.
1.5
1
0.5
0
N LAT clusters / N binding
MCC 14 nm
2C11 14 nm
17A2 14 nm
H57 14 nm
H57 25 nm
H57 50 nm

Figure 5. All short ligands trigger TCR with similar efficiency, while ligands with longer tethers trigger TCR with lower efficiency. (**A**) Snapshots of binding events underneath a T cell (top row) and concurrent image of LAT-eGFP (second row) show that LAT condensates often colocalize with binding events from ligands that create a 14 nm intermembrane space, whereas LAT condensates rarely colocalize with binding events from ligands with longer tethers and there are far fewer LAT condensates in these cells (third and fourth rows). Binding events are colored magenta and LAT is colored green. Scale bar for first three rows 5 μm. Scale bar for zoomed-in region in fourth row 2 μm. (**B**) A single binding event between ligand and TCR is sufficient to create a proximal LAT condensate. The binding event that appears 23 s after cell landing (yellow circle) triggers the formation of a LAT condensate a handful of seconds later. Scale bar 1 μm. (**C**) The numbers of LAT clusters and binding events experienced by cells were counted for the first 2 min after initial cell contact with the bilayer. There is no significant difference in the ratio of the number of LAT clusters to the number of binding events for short ligands. There is a significant decrease in this ratio for ligands with longer DNA tethers. Colored bar: median; black square: mean; box: interquartile range; whiskers: data within 1.5x IQR. Significance was determined by the Mann-Whitney U test (*** $p < 0.001$; **** $p < 0.0001$; n.s. $p > 0.01$) (MCC: n = 11 cells; 2C11 14nm n = 17 cells; 17A2 14nm n = 12 cells; H57 14nm n = 17 cells; H57 25nm n = 16 cells; H57 50nm n = 10 cells). Data are compiled from cells from at least two mice for each condition.